Soft Matter

Programmable soft electrothermal actuators based on free-form printing of the embedded heater

Journal:	*Soft Matter*
Manuscript ID	SM-ART-11-2020-002062.R1
Article Type:	Paper
Date Submitted by the Author:	30-Dec-2020
Complete List of Authors:	Cao, Yang; North Carolina State University Dong, Jingyan; North Carolina State University,

ARTICLE

Programmable soft electrothermal actuators based on free-form printing of the embedded heater

Received 00th January 20xx,
Accepted 00th January 20xx

DOI: 10.1039/x0xx00000x

Yang Cao and Jingyan Dong*

In recent years, there has been an increasing interest in the research of soft actuators that exhibit complex programmable deformations. Soft electrothermal actuators use electricity as the stimulus to generate heat, and the mismatch between the thermal expansions of the two structural layers causes the actuator to bend. Complex programmable deformations of soft electrothermal actuators are difficult due to the limitations of conventional fabrication methods. In this article, we reported a new approach to fabricate soft electrothermal actuators, in which the resistive heater of the electrothermal actuator is directly printed using electrohydrodynamic (EHD) printing. The direct patterning capabilities of EHD printing allow free-form design of the heater. By changing the design of the heater pattern on the actuator, different heat distributions can be achieved and utilized to realize complex programmable deformations, including uniform bending, customized bending, folding, and twisting. The finite element analysis (FEA) was studied to validate the thermal distribution and deformation for different actuator designs. Lastly, several integrated demonstrations are presented, including complex structures obtained from folding, a two-degree-of-freedom soft robot arm, and soft walkers.

Introduction

Soft actuators change their shape or size in response to stimuli like electricity,[1–3] heat,[4,5] light,[6,7] chemical,[8,9] magnetic fields,[10,11] and pneumatic pressure.[12,13] They are lightweight, flexible, and can easily achieve multi-degree-of-freedom motion. Due to their unique characteristics, soft actuators are widely used in biomimetic,[14–16] medical,[17,18] and soft robotic applications.[19–21] When heat is used as the stimulus, it is called a thermal actuator. Thermally responsive soft actuators are usually fabricated in a bimorph structure with two layers that have significant different coefficient of thermal expansion (CTE). When exposed to temperature change from thermal energy, thermal mismatch between the two layers makes the bimorph structure to bend. The thermal energy of the actuator can come from different sources, such as electricity or light, corresponding to electrothermal actuators[22,23] and photothermal actuators,[24,25] respectively. Electrothermal actuators have an electrically conductive heater layer that provides Joule heat during the actuation. Similarly, in photothermal actuators, an active layer containing light absorbing material converts light into heat. Normally, soft actuators exhibit only basic deformations such as expansion, contraction, bending, or folding. In recent years, there has been an increasing trend in the research of soft actuators that achieve complex and programmable deformations.[26–38]

Programmable deformations of soft actuators can be realized in various ways. The first method is through gradient or patterned actuation. Instead of applying a uniform actuation, a gradient of the actuation effect is created on the actuator. For example, the heat absorption ability of photothermal actuators can be regulated by the amount of light-absorbing materials. Chen et al.[26] fabricated a photothermal actuator whose light absorbing layer was toner-coated paper. The amount of black toner (grayscale) printed on the paper can control the absorption ability of light, leading to different temperature and bending curvature of the actuator. Similarly, for chemically responsive actuators that based on the swelling difference between the two structural layers, programmed deformation can be obtained by distributing the relative amount of those two materials. Jeong et al.[27] reported a chemically responsive soft actuator that is triggered by the unbalanced expansion between the two structural layers when immersed in hexane solvent. While a traditional cantilever structure results in bending deformation, an asymmetrical arrangement of two materials on the cross-section of the cantilever results in twisting deformation. Lahikainen et al.[28] realized the patterned deformation of a photo actuator through synergistic use of photochemical and photothermal effects. The photochemical effect is used for patterning the actuator, and the photothermal effect is used for triggering actuation. With mask patterned ultraviolet exposure, the azobenzene crosslinks in the actuator undergo trans-cis isomerization, which leads to patterned bending deformation under red light irradiation. Ma et al.[29] fabricated a moisture-responsive graphene actuator that has programmable shape-changing capability by patterning its SU-8

Edward P Fitts Department of Industrial and Systems Engineering, North Carolina State University, Raleigh, NC 27695, USA. E-mail: jdong@ncsu.edu

† Electronic Supplementary Information (ESI) available: Uniform bending, folding, and twisting deformation images and FEA simulation results (pdf), Video S1: folding deformation, Video S2: twisting deformation, Video S3: soft robot arm, Video S4: soft walker on ratchet surface, Video S5: bidirectional soft walker on flat surface. See DOI: 10.1039/x0xx00000x

layer through ultraviolet lithography. By controlling the geometries and orientations of the SU-8 micropattern arrays, the actuator can achieve complex deformations, including bending, twisting, coiling, etc.

Another way for soft actuators to realize complex programmable deformations is by controlling their deformation direction. This is especially true for twisting deformation, as twisting deformation can be obtained from a bending deformation that is misaligned with the long axis of the actuator. For soft pneumatic network actuators, this can be done by orienting the air chambers by an angle from the transverse direction.[30] Some photo responsive materials exhibit uniaxial deformation or have a dominant deformation direction. For example, Hu et al.[31] reported a photo actuator which was fabricated by compositing a photo-liquefiable azobenzene derivative with polyethylene film. Guided rubbing and annealing treatments were subsequently applied to the composite film. Actuators obtained by cutting along the rubbing direction exhibited only bending deformation, while actuators obtained by cutting at an angle with the rubbing direction exhibited helical twisting. Wang et al.[32] developed a dual-layer liquid crystal soft actuator that can bend under ultraviolet irradiation and twist under near-infrared irradiation. The top layer possesses a uniaxially aligned liquid crystalline elastomer matrix incorporated with azobenzene chromophores and a near-infrared absorbing dye, so it bends under ultraviolet stimulus and shrinks under near-infrared stimulus. The bottom layer has only near-infrared dye, and only responds to near-infrared stimulus. Because the shrinkage directions of the top and bottom layers are tilted to each other, the actuator executes twisting deformation under near-infrared irradiation. For magnetic soft actuators, programmable deformation can be achieved by rearranging the magnetization patterns and directions. Song et al.[33] fabricated a soft magnetic actuator that was composed of spatially separated magnetic microspheres encapsulated in oligomeric polyethylene glycol. Solid-to-liquid phase transition of this encapsulating oligomer allows rearrangement of the magnetization directions in the magnetic microspheres. At a lower temperature, the magnetization directions of the magnetic microspheres are fixed; while at a higher temperature, the magnetization directions can be rearranged to any desired form under external magnetic fields. Besides, humidity responsive actuators based on uniaxially aligned liquid crystal polymer network[34] and thermal responsive hydrogel fibrous membranes showing directionally controlled movements[35] were also reported.

Programmable deformations of soft actuators can also be achieved by mechanical anisotropy. For an actuator strip, its bending deformation tends to occur along the direction that has the lowest bending stiffness. If that direction is misaligned with the transverse direction, a twisting deformation will be produced in addition to the bending deformation. Bending stiffness patterns are commonly altered by reinforcements like reinforcing stripes, fibers, and wires. For example, Schaffner et al.[36] reported a 3D printed pneumatic soft actuator that can bend, contract, twist, and grab by designing the tube shape and configuring its reinforcing stripes. Wang et al.[37] designed a thermal responsive soft actuator that exhibited coupled twisting and bending deformation, which comes from its structure anisotropy induced by the embedded shape memory polymer fibers in a homogeneous elastic matrix. Similarly, Song et al.[38] developed a shape memory alloy actuator that can achieve coupled bending-twisting actuation by embedding an anisotropic layered reinforcement structure.

Programmable deformations of soft electrothermal actuators are challenging, mainly restricted by the free-form fabrication capabilities of the resistive heater. Most soft electrothermal actuators reported so far utilize the deposition (e.g., spin-coating,[39] casting,[40] filtration,[41] spray[42]) of nanomaterial-based solution to form a thin conductive heater layer with only uniform heating capability, which is difficult to provide customized actuation and temperature distribution. Unlike these previously reported soft electrothermal actuators, in this work, the custom programmed heater is fabricated in the actuator, which is directly printed with pre-designed patterns using the electrohydrodynamic (EHD) printing technology. The direct fabrication capabilities from EHD printing enable free-form design of the embedded heater, which can easily control the heated area and the temperature distribution, leading to complex programmable deformations like uniform bending, customized bending, folding, and twisting. To the best of our knowledge, this is the first soft electrothermal actuator reported to have achieved programmable bending and twisting deformations. These different modes of deformation were validated using experiments and finite element analysis (FEA) in ANSYS and were integrated for various demonstrations like controlled structure formation, a soft robot arm, and soft walkers.

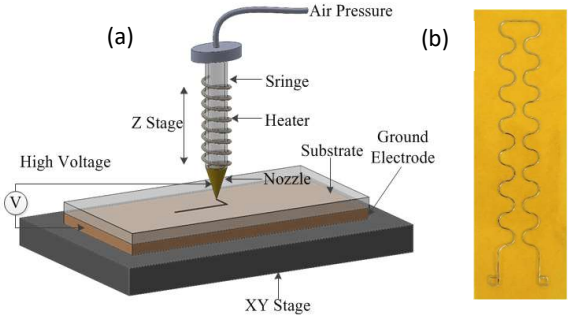

Fig. 1 (a) Schematic of the EHD printing system. (b) An EHD printed heating filament using the low melting point metal alloy.

Results and discussion

The EHD printing system and process

EHD printing is a maskless patterning technology that uses an electric field to induce fluid flows from micro capillary nozzles.[44,45] An EHD printing process was developed to print the low melting point alloy with high resolution into fine filaments as the resistive heater. The direct patterning capabilities of EHD printing enable customized design and fabrication of the embedded heater for the soft actuator. The EHD printing

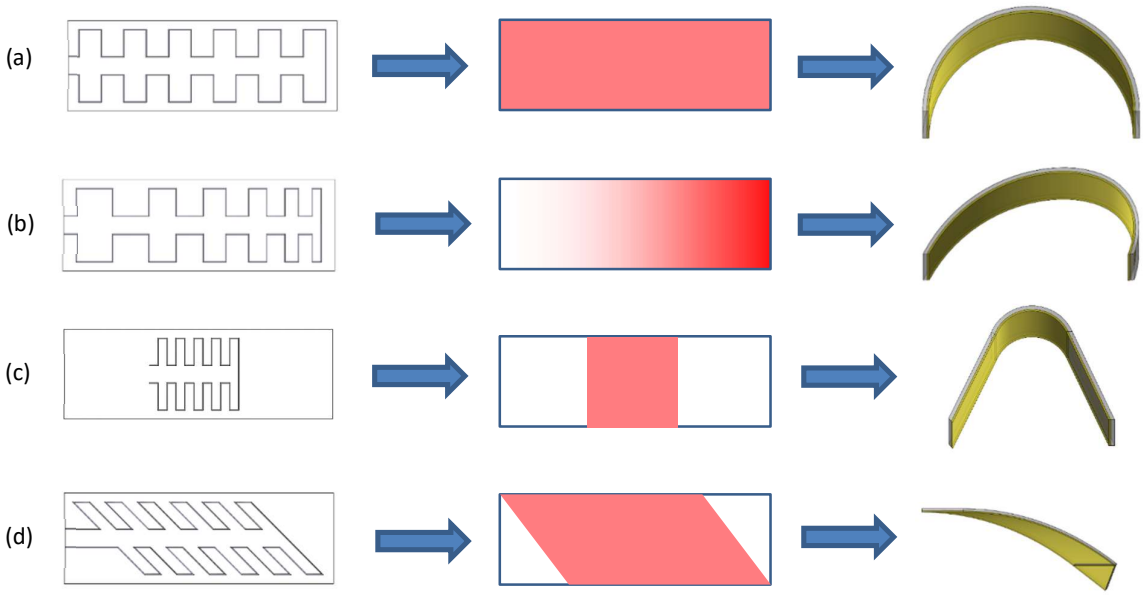

Fig. 2 Schematic design of programable actuators with different heater patterns, temperature distributions on the actuator when supplied with voltage, and the corresponding deformation for (a) uniform bending, (b) customized bending, (c) folding, and (d) twisting.

system used in this study (Fig. a) consists of a three-axis motion stage, a temperature-controlled syringe, a high voltage supply, and a pneumatic dispensing system. The motion stage, directed by computer numerical control (CNC) program, can move in XYZ directions with high resolution. The low melting point metal ink is melted in the heated syringe and flowed to the nozzle tip by a small pneumatic pressure. When a high voltage is applied between the nozzle and the grounded substrate, the resulting electrostatic force overcomes surface tension of the ink, deforms the meniscus at the nozzle tip into a conical shape (called Taylor cone), and ejects a fine filament with its size smaller than the nozzle's diameter. Using the programmed printing path, the customized heater can be directly printed, as shown in Fig. 1b. The detailed printing parameters are provided in the Materials and methods section.

Design concept of the programmable electrothermal actuator

The programmable soft electrothermal actuator is fabricated in a sandwich structure. The two structural layers are polydimethylsiloxane (PDMS) and polyimide (PI), which are selected due to the large difference in their CTEs. A heater is embedded in between these two layers, which is directly printed by EHD printing using a low melting point alloy Bi58/Sn42 (58% Bismuth, 42% Tin). When supplied with electricity, the resistive heat generated by the heater changes the temperature of the actuator. The large mismatch between the thermal expansions of the two structural layers causes the actuator to deform. Fig. shows the design concept of the programmable electrothermal actuator, which can realize four different modes of deformation: uniform bending, customized bending, folding, and twisting, by customizing the heater design and the resulting temperature distribution. In Fig.a, the heater is printed to cover the actuator uniformly by a zigzag pattern with equal line spacing. When a voltage is applied, it generates an evenly heated area that leads to uniform bending. Fig.b shows a heater pattern whose line spacing is reduced from left to right. This heater design generates a gradient heating area, and the resulting temperature field gradually increases from left to right, which results in bending deformation with customized curvature. By localized heating, folding deformation as in the traditional rotary joint can be obtained, as shown in Fig.c, since the polymeric structural materials are not good heat conductors. Furthermore, the heater filaments can also be custom printed along a direction that has an angle with the transverse direction as shown in Fig.d. This oblique heater design not only creates a skewed parallelogram high temperature zone, but also changes the stiffness anisotropy of the actuator. The actuator tends to bend along the direction of the temperature field with lower bending stiffness, which is now parallel to the oblique heater filaments. This skewed bending produces twisting deformation with parasitic bending.

Uniform bending

Uniform bending of the actuator can be achieved when the embedded heater is uniformly patterned on the actuator, as shown in Fig. a. When an actuation voltage is applied, a roughly uniform temperature distribution is obtained for the actuator as shown in the thermography of Fig. b. Since for the electrothermal actuator, the bending curvature is proportional to its temperature increasement, uniform temperature distribution results in a constant bending curvature and bending radius. Fig. c shows the actuator's bending profile when the supply voltage is 3.5 V, in which a circular bending deformation is achieved with a constant radius. The bending curvature of the actuator can be easily controlled by the actuation voltage and the resulting heating temperature, and the bending curvature generally follows a linear relationship with the temperature

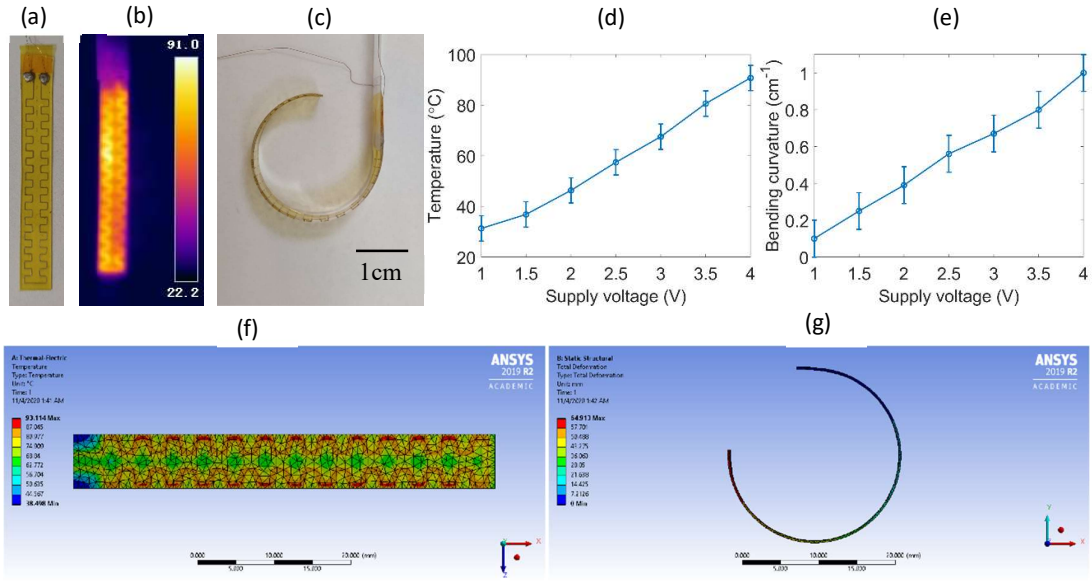

Fig. 3 Uniform bending. (a) The fabricated actuator and heater pattern; (b) Thermography of an actuated actuator; (c) Uniform bending deformation of an actuator; (d) The stable average temperature achieved at different actuation voltages; (e) The bending curvature at different voltages; (f) FEA simulation of the temperature distribution by thermal analysis; (g) Deformation of the actuator from FEA analysis.

change from the theoretical equation of bimorph structure[43] and was demonstrated in our previous study.[23]

$$\kappa = \frac{6(\alpha_2 - \alpha_1)(1+m)^2}{h(3(1+m)^2 + (1+mn)(m^2 + 1/mn))}\Delta T \qquad (1)$$

where κ is the curvature, α_1 and α_2 are CTEs of the materials in two layers, t_1, t_2 are the thickness of the two layers, $h = t_1 + t_2$, $m = t_1 / t_2$, E_1 and E_2 are Young's modulus of the two layers, and $n = E_1 / E_2$, ΔT is the temperature change. Fig. d and 3e show the actuator's stable average temperature and bending curvature at different voltages, respectively. In both diagrams, a linear trend can be clearly observed. Moreover, an electric-thermal-mechanical finite element model was developed to study the temperature distribution and the deformation of the actuator and to verify each specific heater design. The FEA simulation results from the corresponding thermal analysis and deformation analysis, as shown in Fig. f and 3g, agree well with the experimental results. Images of the uniform bending deformation and FEA simulation results at different voltages are provided in Fig. S1 (ESI†).

Customized bending

The direct fabrication capabilities of EHD printing enable free-form customized design of the embedded heater, which makes

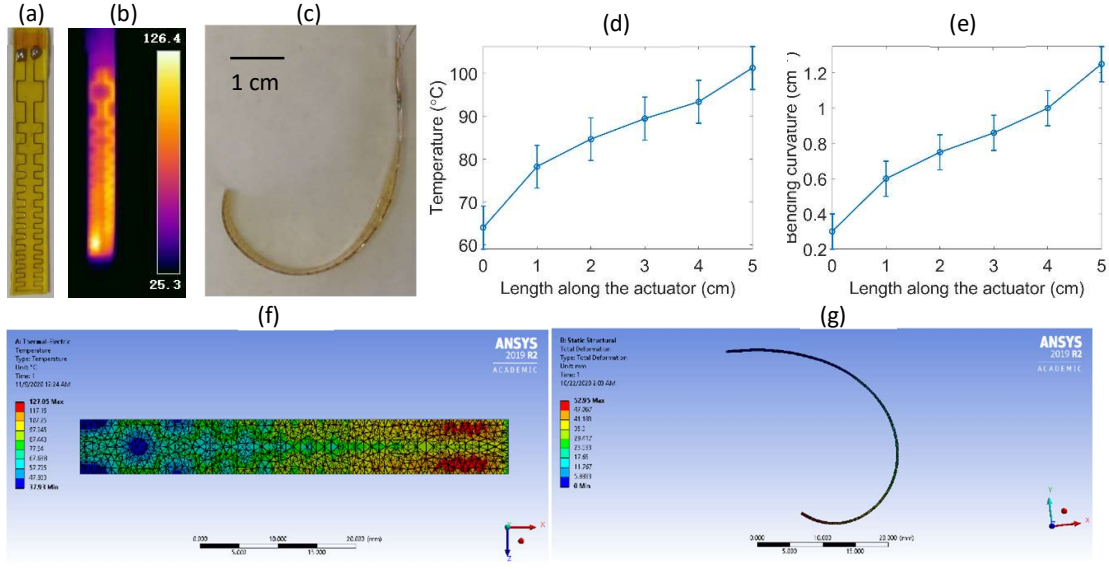

Fig. 4 Customized bending. (a) The fabricated actuator and heater pattern; (b) Thermography of an actuated actuator; (c) Customized bending deformation; (d) The average temperature at different locations along the actuator; (e) The bending curvature at different locations along the actuator; (f) FEA simulation of the temperature distribution by thermal analysis; (g) Deformation of the actuator from FEA analysis.

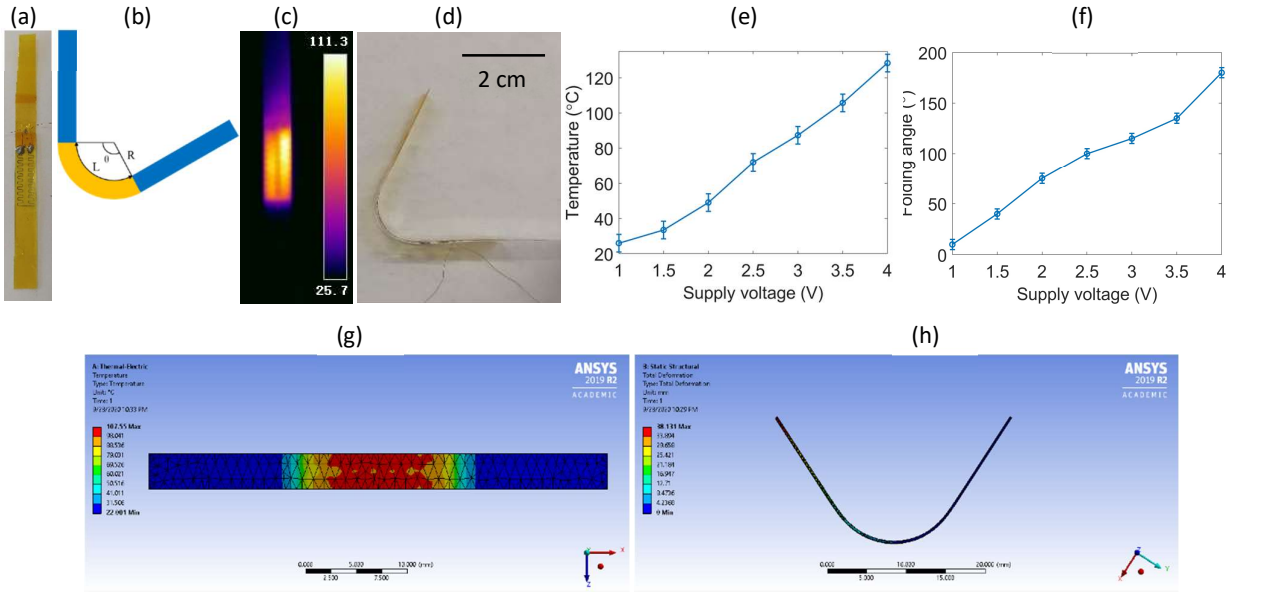

Fig. 5 Folding. (a) The fabricated actuator and heater pattern; (b) Schematic of the folding structure; (c) Thermography of an actuated actuator; (d) Folding deformation of the actuator under actuation; (e) The average temperature on the folding joint at different voltages; (f) The folding angle achieved at different voltages; (g) Temperature distribution by FEA thermal analysis; (h) Deformation of the actuator from FEA analysis.

it possible to program the temperature distribution on the actuator, such as a temperature gradient. For example, in Fig. a, a soft actuator with a continuous change of the temperature field and the resulting programmed bending curvature was fabricated and tested. The line spacing of the heater filaments decreases and the heater filament density increases from top to bottom. Because of the equal electric current flowing through the heater filament and the almost uniform diameter of the heater filament, the area density of the heating power is determined by the area density of the heater filament. Due to the changing line spacing, the area with narrower line spacing has a denser heater filament distribution, and naturally a higher average temperature (as shown in Fig. b) and a larger bending curvature. Fig. c shows the actuator's profile when a 4 V voltage is applied. The average temperature and bending curvature at different locations along the actuator from top to bottom were measured and shown in Fig. d and 4e, respectively. Clearly a temperature gradient can be observed on the actuator because of the different density in the heating filament. A gradually changing bending curvature can also be observed, which follows the same trend with the temperature gradient on the actuator. The FEA simulation results on the temperature distribution and the corresponding actuator deformation at the same actuation voltage of 4V are shown in Fig. f and 4g. The deformation profile of the actuator from FEA is very close to that from the experimental result in Fig. c. With the assistance of the FEA model and the experimental data, it is possible to design and fabricate an actuator that can bend to a customized bending profile.

Folding

Folding provides localized bending that is similar to the traditional rotary joint. Folding enables kinematically precise rotary degree-of-freedom for mechanism design in soft robotics. Another widely studied application of soft actuators is their abilities to form customized structures by folding of 2D sheets. The folding can be realized by locally heating the actuator to an enough extent. As shown in Fig. a, on an actuator strip, only the middle area is printed with heater filaments. As shown in Fig. b, when the middle area is heated to a certain bending curvature, the folding angle can be calculated by the following formula:

$$\theta = \frac{L}{R} = L\kappa \qquad (2)$$

in which θ is the folding angle, L is length of the localized heating area, R and κ are the bending radius and curvature, respectively. Therefore, the folding angle can be controlled by either the actuator length or the bending curvature which can be regulated by the supplied actuation voltage.

Fig. c shows the thermography of the actuator at a voltage of 3 V. As it can be observed from the thermal image, the actuator has a locally heated area, since the structural materials both have relatively low thermal conductivity. From the deformation of the actuator, a clear folding is observed, as shown in Fig. d. The relationship of the stable average temperature on the folding joint and the folding angle with respect to different actuation voltages are shown in Fig. e and 5f, which indicate a rough linear relationship. The folding deformation was also analysed using FEA tool, as shown in Fig. g and 5h, corresponding to the thermal analysis and deformation analysis. Experimental folding deformation and FEA results at different voltages are provided in Fig. S2 (ESI†), which agree well qualitatively, and Video S1 (ESI†) shows the folding deformation process.

Twisting

Twisting deformation of the electrothermal actuator can be realized by printing a skewed heater pattern as shown in Fig. a.

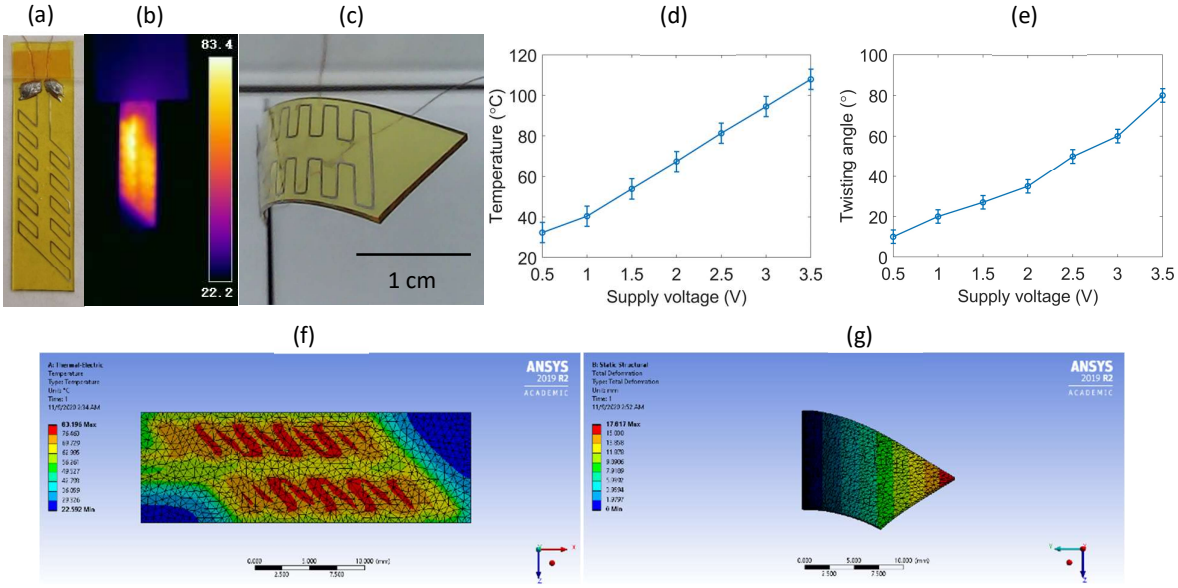

Fig. 6 Twisting. (a) The fabricated actuator and heater pattern; (b) Thermography of an actuated actuator; (c) Twisting deformation from the actuator; (d) The average temperature achieved at different voltages; (e) The twisting angle at different voltages; (f) Temperature distribution by FEA thermal analysis; (g) Deformation of the actuator from FEA analysis.

This oblique heater can not only generate a parallelogram high-temperature zone as shown in Fig. b, but also changes the stiffness anisotropy of the actuator. For the uniform bending, the transverse direction has the lowest bending stiffness. While for the skewed heater pattern, the heating area and the direction with the lowest bending stiffness shift to be parallel to the skewed heater filaments. The actuator tends to bend along this oblique direction, resulting in a twisting deformation with parasitic bending as shown in Fig. c with the voltage applied of 2.5 V. We have measured the stable average temperature on the actuator and the twisting angle at different actuation voltages, as shown in Fig. d and 6e, respectively. A linear relationship is observed between the actuation voltage and the resulting twisting angle from the actuator. Note that the actuator in Fig. has a clockwise twisting deformation. A counterclockwise twisting motion can also be obtained when the heater filament skewing angle is oriented to the other side. Fig. f and 6g show the FEA simulation results for thermal analysis and deformation analysis, which agree very well with the experimental results. Experimental twisting deformation and FEA results at different voltages are provided in Fig. S3 (ESI†), which shows good agreement, and Video S2 (ESI†) shows the twisting deformation process.

Applications of the programmable soft actuator

The soft actuators with programable deformation have many potential applications such as soft robotics and micro assembly. In this work, we studied a few typical applications of the programable soft actuator in controlled structure formation, multiple degree of freedom mechanism, and soft walking robots.

By configurating multiple actuators together, different structures can be formed in a controlled way by selecting folding joints with different rotary directions. Two folding structures were obtained as shown in Fig. a and 7b from a straight strip under actuation. The folding actuators can be used as folding joints with their folding angles being controlled by the actuation voltage. The actuators were joined together using connection materials (PI tape and polyethylene terephthalate or PET sheets). In Fig. a, both actuators have their PI side faced up. By controlling both folding angles to 120 °, a triangle structure can be obtained. In Fig. b, one folding actuator has PDMS side up, and the other has PI side up, thus giving them inverse rotational directions. By controlling both folding angles to 90 ° using the actuation voltage, a Z shape structure can be achieved.

Our programmable actuators have been realized to achieve different types of motion. Actuators can be put together and utilized to realize a multi-degree-of-freedom soft robot arm as shown in Fig. c. Two actuators (one bending actuator and one twisting actuator) were connected to mimic a soft robot arm, which has two degree-of-freedom: lifting motion and twisting motion. When the bending actuator is powered on, it lifts the structure up (as shown from Fig. d to 7e). When the twisting actuator is powered on, the arm tip twists (as shown from Fig. e to 7f). These two motions can be controlled independently or collaboratively with lifting distance and twisting angle being controlled separately. Video S3 (ESI†) shows operation of the two joints of the soft robot arm.

Self-walking is the basic motions of robots. Unlike the complex electromechanical system in conventional rigid walking robots, soft actuators can walk using the biomimetic worm-like crawling motion. We developed a prototype soft walking robot using a single electrothermal actuator, as shown in Fig. a. A relatively rigid copper tape was attached to the middle of the actuator strip to form a local curve, which facilitates the contraction and relaxation motions of the actuator. A ratchet walking surface was prepared by stacking a pile of paper cards. This asymmetrical ratchet structure allows the soft robot to proceed one-directional walking motion when

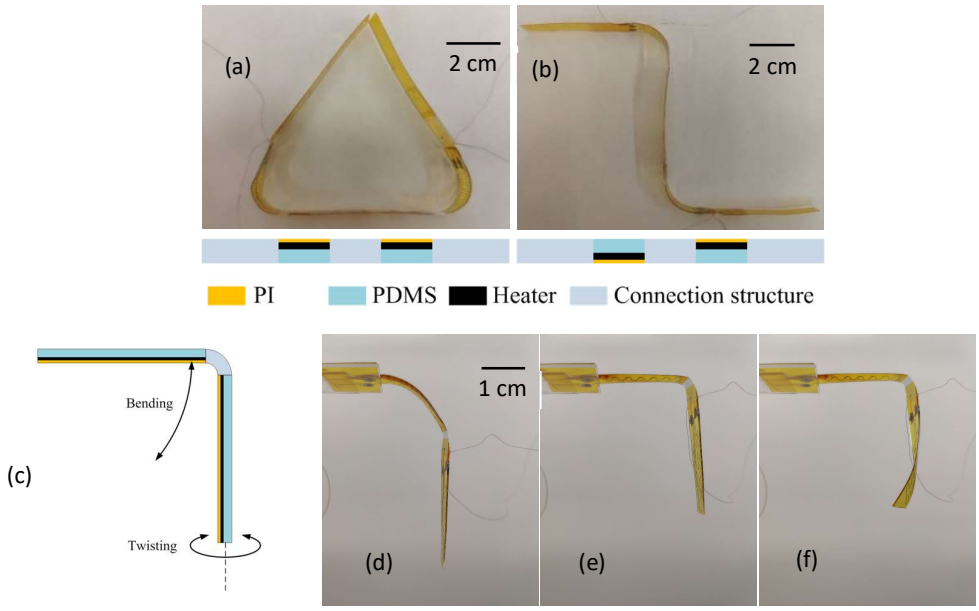

Fig. 7 Controlled structure formation and a two-degree-of-freedom soft robot arm. (a) A triangle structure and (b) A Z-shape structure obtained from a straight strip after actuation. (c) Schematic of a two-degree-of-freedom soft robot arm. The soft robot arm at (d) Unactuated state, (e) Lifting applied, (f) Twisting applied.

supplied with periodic pulses of voltage signal. We used a 40 s periodic voltage signal (20 s ON and 20 s OFF, shown in Fig. b) to drive the soft walking robot. Fig. c shows the profile and position of the soft walker at different time moments. In the contraction stage (voltage was ON), the rear leg slid forward, while the front leg was mostly restricted from sliding backward by the ratchet structure (from 0 to 20 s). Similarly, in the relaxation stage (voltage was OFF), the front leg slid forward while the rear leg was kept at the same position by the ratchet face (from 20 to 40 s). The repeated contraction and relaxation motions of the actuator can be converted into forward walking. In 3 minutes, it moved to right by 15 mm (shown in 180 s), indicating a walking velocity about 5 mm/min. Video S4 (ESI†) shows walking of the soft robot on the ratchet surface.

The soft walker on the ratchet surface only provides one-directional walking motion. Integrating flexibly fabricated programable actuators, we further developed a soft walker that can walk both forward and backward on a flat surface. As shown in Fig. 9a, instead of using a single actuator, this soft walker is consisted of two actuators linked together but functioning independently. Moreover, a foot in the middle of the soft walker was used as a support. The soft walker was placed on a table surface and three markers were used to denote the initial positions of the two actuator tips as well as the middle foot. By controlling the commands on the two actuators, bi-directional walking motion can be achieved. Fig. 9d shows the profile and position of the soft walker at different time moments. For one walk cycle, at the beginning, when both actuators were actuated, the two actuators contracted inward and lifted the

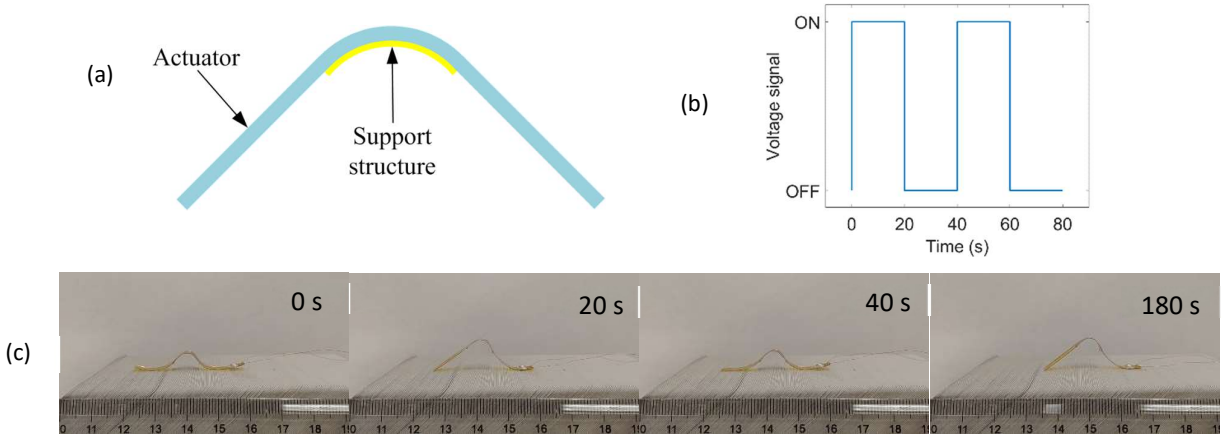

Fig. 8 Demonstration of the electrothermal actuator as a soft walker on a ratchet surface. (a) Schematic of the soft walker from a single actuator; (b) Voltage signal of the actuator; (c) Successive profiles of the soft walker crawling on a ratchet surface.

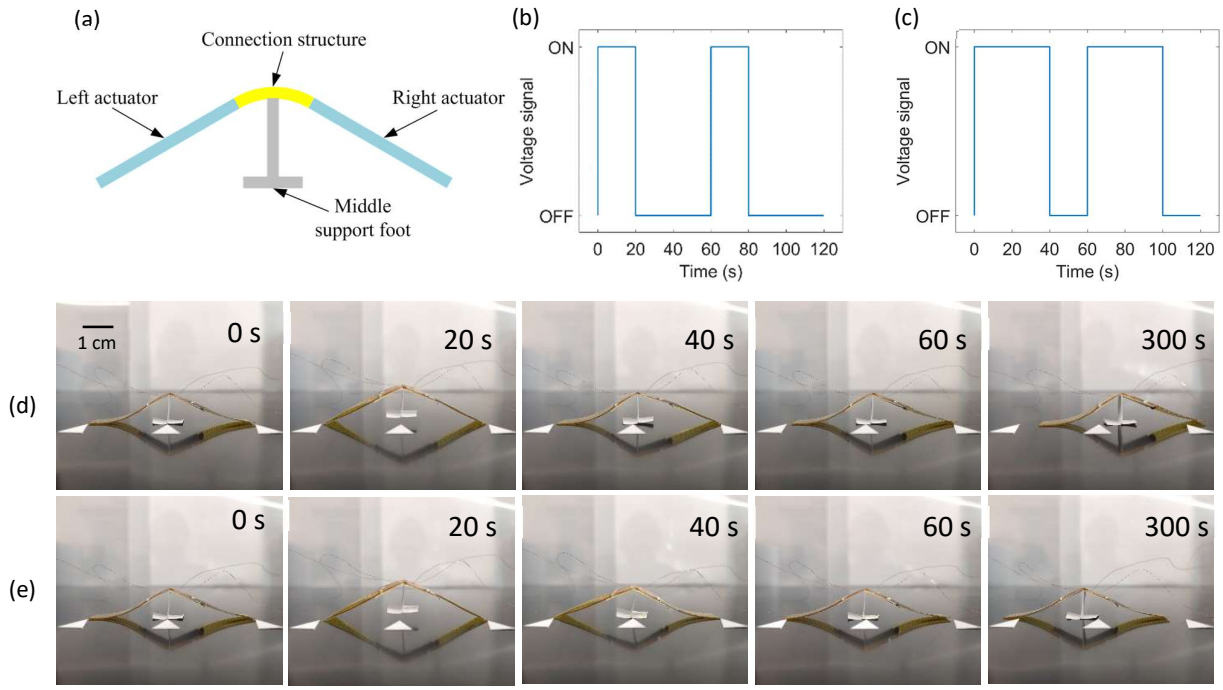

Fig. 9 Demonstration of the electrothermal actuators as a bidirectional soft walker on a flat surface. (a) Schematic of the soft walker with two actuated legs and the middle support foot; (b) Voltage signal on the left actuator when proceeding to right; (c) Voltage signal on the right actuator when proceeding to right; (d) Successive profiles of the bidirectional soft walker proceeding to right; (e) Successive profiles of the bidirectional soft walker proceeding to left.

middle foot up (from 0 to 20 s). At the next step, the voltage for the left actuator was first cut off. The left actuator bent downward and pushed the middle foot rightward slightly (from 20 to 40 s). Then, the voltage for the right actuator was cut off, and the whole structure moved a step toward right (from 40 to 60 s). This gait pattern can be repeated using a periodic pulse. A one-minute cyclic signal (both actuators ON for 20 s, left OFF for 20 s and right OFF for 20 s) was used to control the walking motion. The voltage signals for the left actuator and the right actuator are shown in Fig. 9b and 9c, respectively. After executing 5 full cycles, the soft walker moved to the right about 10 mm, indicating a walking speed about 2 mm/min. Video S5 (ESI†) shows walking of the bidirectional soft walker on the flat surface. By changing the control signals on the two actuators, motion in the other direction can also be achieved. When the voltage signals are changed to that the right actuator is turned off first and then the left actuator is turned off, the soft walker can also walk toward left direction in a similar gait mode (shown in Fig. 9e).

Conclusions

In this paper, we reported soft electrothermal actuators that exhibit complex programmable deformations. The programmable deformation was achieved through the configuration of the embedded heater and the resulting temperature distribution field on the actuator. Unlike most conventional deposition methods used to fabricate electrothermal actuators, we used EHD printing to directly print the embedded heater. The direct patterning capabilities of EHD printing allow free-form design of the heater pattern. A uniformly patterned heater can generate an evenly heated area and hence a uniform bending. The heater pattern with varied line spacing creates a heating gradient, which leads to a bending deformation with changing curvature. The localized heater pattern causes a localized heating area and hence produces a folding deformation as a rotary joint. The skewed heater pattern creates a parallelogram heating area, which results in twisting deformation with parasitic bending. These programable actuator designs and their deformation modes were validated by FEA using thermal analysis and deformation analysis. Lastly, the soft actuators with these different deformation modes were integrated for different applications and demonstrations, including controlled structure formation, a two-degree-of-freedom mechanism for a soft robot arm, and soft walkers.

Materials and methods

Materials

The PI tape was purchased from CAPLINQ with 0.5 mil (12.7 µm) thickness PI and 1 mil (25.4 µm) thickness silicone adhesive. PDMS (Sylgard 184) was purchased from the Dow Chemical Company. The base and curing agent were mixed by a ratio of 10:1 as suggested. PDMS was adequately agitated and degassed for an hour before casting. The printing alloy used for the heater filaments was Bi58/Sn42 (58% Bismuth and 42% Tin), which was

a solder wire purchased from Qualitek International Inc. All materials were used as received.

The EHD printing process

To print the low melting point alloy Bi58/Sn42, the alloy was loaded into the syringe and melted at a printing temperature 260 °C to achieve good ink flowability under a pneumatic pressure 0.1 to 0.2 psi (689 to 1379 Pa). A printing nozzle with inner diameter 0.234 mm was used for the EHD printing process. A printing voltage about 2 kV was applied between the nozzle and a conductive ground electrode below the substrate. With a printing speed ranging from 0.5 to 1 mm/s, different heater patterns were printed onto the substrate using the programmed printing toolpath.

Fabrication of the electrothermal actuator

To prepare a suitable substrate for EHD printing, a layer of PDMS was first coated on a glass slide. After the PDMS fully cured, the microfilament heater was printed on the PDMS substrate by EHD printing. Then a PI tape was pressed against the heater to peel the heater filament off from the PDMS. Thereafter, copper wires were connected to the printed heater using solder for connection to the power supply. Finally, a layer of PDMS was coated onto the microfilament heater and the PI layer with controlled PDMS layer thickness. When the top PDMS layer was fully cured, the actuator was produced by cutting the bimorph film into designed sizes. The fabricated actuators showed stable and consistent cyclic operations in experiment.

Temperature, curvature, and angle measurement

The temperature of the electrothermal actuators was measured using an infrared camera (Fotric 225). The profile of the actuator was captured using a digital camera, then its bending curvature was measured by the best fitted circle. For the customized bending shown in Fig. , the actuator profile was divided into several segments along its length, then bending curvature of each segment was measured individually by the best fitted circle. Folding and twisting angles were measured by a protractor with 1 ° resolution.

Conflicts of interest

There are no conflicts to declare.

Acknowledgements

The authors would like to acknowledge the financial support from the National Science Foundation (NSF) through Award CMMI 1728370.

References

1 K. Jun, J. Kim and I. K. Oh, Small, 2018, **14**, 35, 1801603.
2 G. K. Lau, T. G. La, E. S. W. Foong and M. Shrestha, Smart Mater. Struct., 2016, **25**, 125006.
3 V. Palmre, E. Lust, A. Janes, M. Koel, A. L. Peikolainen, J. Torop, U. Johanson and A. Aabloo, J. Mater. Chem., 2011, **21**, 2577–2583.
4 T. H. Kim, J. G. Choi, J. Y. Byun, Y. Jang, S. M. Kim, G. M. Spinks and S. J. Kim, Sci. Rep., 2019, **9**, 7905.
5 H. Y. Jeong, E. Lee, S. Ha, N. Kim and Y. C. Jun, Adv. Mater. Technol., 2019, **4**, 1800495.
6 C. L. Huang, J. A. Lv, X. J. Tian, Y. C. Wang, Y. L. Yu and J. Liu, Sci. Rep., 2015, **5**, 17414.
7 J. A. Lv, W. Wang, W. Wu and Y. L. Yu, J. Mater. Chem. C, 2015, **3**, 6621–6626.
8 Q. Zhao, J. W. C. Dunlop, X. L. Qiu, F. H. Huang, Z. B. Zhang, J. Heyda, J. Dzubiella, M. Antonietti and J. Y. Yuan, Nat. Commun., 2014, **5**, 4293.
9 J. Y. Park, H. J. Oh, D. J. Kim, J. Y. Baek and S. H. Lee, J. Micromech. Microeng., 2006, **16**, 656–663.
10 M. M. Schmauch, S. R. Mishra, B. A. Evans, O. D. Velev and J. B. Tracy, ACS Appl. Mater. Interfaces, 2017, **9**, 11895–11901.
11 R. Fuhrer, E. K. Athanassiou, N. A. Luechinger and W. J. Stark, Small, 2009, **5**, 383–388.
12 T. Sun, Y. L. Chen, T. Y. Han, C. L. Jiao, B. B. Lian and Y. M. Song, Robot. Comput.-Integr. Manuf., 2020, **61**, 101848.
13 L. S. Ge, L. T. Dong, D. Wang, Q. Ge and G. Y. Gu, Sens. Actuator A-Phys., 2018, **273**, 285–292.
14 A. W. Feinberg, A. Feigel, S. S. Shevkoplyas, S. Sheehy, G. M. Whitesides and K. K. Parker, Science, 2007, **317**, 1366–1370.
15 A. E. Aliev, J. Y. Oh, M. E. Kozlov, A. A. Kuznetsov, S. L. Fang, A. F. Fonseca, R. Ovalle, M. D. Lima, M. H. Haque, Y. N. Gartstein, M. Zhang, A. A. Zakhidov and R. H. Baughman, Science, 2009, **323**, 1575–1578.
16 Y. Hu, T. Lan, G. Wu, Z. C. Zhu and W. Chen, Nanoscale, 2014, **6**, 12703–12709.
17 S. Mura, J. Nicolas and P. Couvreur, Nat. Mater., 2013, **12**, 991–1003.
18 H. J. Jiang, M. Ochoa, J. F. Waimin, R Rahimi and B Ziaie, Lab Chip, 2019, **19**, 2265–2274.
19 W. J. Zheng, N. An, J. H. Yang, J. X. Zhou and Y. M. Chen, ACS Appl. Mater. Interfaces, 2015, **7**, 1758–1764.
20 P. S. Xiao, N. B. Yi, T. F. Zhang, Y. Huang, H. C. Chang, Y. Yang, Y. Zhou and Y. S. Chen, Adv. Sci., 2016, **3**, 1500438.
21 R. F. Shepherd, F. Ilievski, W. Choi, S. A. Morin, A. A. Stokes, A. D. Mazzeo, X. Chen, M. Wang and G. M. Whitesides, Proc. Natl. Acad. Sci. U. S. A., 2011, **108**, 20400–20403.
22 S. S. Yao, J. X. Cui, Z. Cui and Y. Zhu, Nanoscale, 2017, **9**, 3797–3805.
23 Y. Cao and J. Y. Dong, Sens. Actuator A-Phys., 2019, **297**, 111546.
24 Leeladhar, P. Raturi, A. Kumar and J. P. Singh, Smart Mater. Struct., 2017, **26**, 095030.
25 Leeladhar, P. Raturi and J. P. Singh, Sci. Rep., 2018, **8**, 3687.
26 L. Z. Chen, M. C. Weng, F. Huang and W. Zhang, Sens. Actuator B-Chem., 2019, **282**, 384–390.
27 K. U. Jeong, J. H. Jang, D. Y. Kim, C. Nah, J. H. Lee, M. H. Lee, H. J. Sun, C. L. Wang, S. Z. D. Cheng and E. L. Thomas, J. Mater. Chem., 2011, **21**, 6824–6830.
28 M. Lahikainen, H. Zeng and A. Priimagi, Nat. Commun., 2018, **9**, 4148.
29 J. N. Ma, Y. L. Zhang, D. D. Han, J. W. Mao, Z. D. Chen and H. B. Sun, Natl. Sci. Rev., 2020, **7**, 775–785.
30 T. Y. Wang, L. S. Ge and G. Y. Gu, Sens. Actuator A-Phys., 2018, **271**, 131–138.
31 J. Hu, X. Li, Y. Ni, S. D. Ma and H. F. Yu, J. Mater. Chem. C, 2018, **6**, 10815–10821.

32 M. Wang, B. P. Lin and H. Yang, Nat. Commun., 2016, **7**, 13981.
33 H. Song, H. Lee, J. Lee, J. K. Choe, S. Lee, J. Y. Yi, S. Park, J. W. Yoo, M. S. Kwon and J. Kim, Nano Lett., 2020, **20**, 5185–5192.
34 L. T. de Haan, J. M. N. Verjans, D. J. Broer, C. W. M. Bastiaansen and A. P. H. J. Schenning, J. Am. Chem. Soc., 2014, **136**, 10585–10588.
35 L. Liu, S. H. Jiang, Y. Sun and S Agarwal, Adv. Funct. Mater., 2016, **26**, 1021–1027.
36 M. Schaffner, J. A. Faber, L. Pianegonda, P. A. Ruhs, F. Coulter and A. R. Studart, Nat. Commun., 2018, **9**, 878.
37 D. Wang, L. Li, B. Zhang, Y. F. Zhang, M. S. Wu, G. Y. Gu and Q. Ge, Int. J. Solids Struct., 2020, **199**, 169–180.
38 S. H. Song, J. Y. Lee, H. Rodrigue, I. S. Choi, Y. J. Kang and S. H. Ahn, Sci. Rep., 2016, **6**, 21118.
39 W. Sang, L. M. Zhao, R. Tang, Y. P. Wu, C. H. Zhu and J. Liu, Macromol. Mater. Eng., 2017, **302**, 1700239.
40 Y. C. Sun, B. D. Leaker, J. E. Lee, R. Nam and H. E. Naguib, Sci. Rep., 2019, **9**, 11445.
41 C. W. Wang, Y. B. Wang, Y. G. Yao, W. Luo, J. Y. Wan, J. Q. Dai, E. Hitz, K. Fu and L. B. Hu, Adv. Mater., 2016, **28**, 8618–8624.
42 J. Ahn, Y. Jeong, Z. J. Zhao, S. Hwang, K. Kim, J. Ko, S. Jeon, J. Park, H. Kang, J. H. Jeong and I. Park, Adv. Mater. Technol., 2020, **5**, 1900997.
43 S. Timoshenko, J. Opt. Soc. Am. Rev. Sci. Instrum., 1925, **11**, 233–255.
44 Y. W. Han and J. Y. Dong, J. Manuf. Syst., 2018, **48**, 24–29.
45 Y. W. Han and J. Y. Dong, Adv. Mater. Technol., 2018, **3**, 1700268.